

Laminar Film Flow Along a Periodic Wall

V. Bontozoglou¹

Abstract: Laminar, gravity-driven flow of a liquid down an inclined wall with large-amplitude sinusoidal corrugations is studied numerically by a spectral spatial discretization method. The synchronous resonance between the wall and the free surface is investigated for corrugations with wavelength 0.002 m , which – according to linear theory – lead to strongest interaction. Free surface profile and flow structure are studied as a function of the film Reynolds number and the wall amplitude. Streamline patterns are computed and conditions leading to flow reversal are established. The distribution of the shear stress along the wall and of the normal velocity gradient close to the free surface are computed and related to heat/mass transport.

keyword: wavy wall, film flow, resonance

1 Introduction

Gravity-driven flow of a liquid film along a plane wall is an intensely studied subject. The linear stability characteristics of this flow have been addressed in numerous investigations [Benjamin (1957); Yih (1963); Benney (1966)]. Recent efforts have focused on the understanding of nonlinear dynamics [for a review see Chang (1994)]. A much less studied problem involves film flow along a periodic, wavy wall. Practical motivation is provided by the extensive application of “modified” surfaces in process equipment, aiming at enhancing heat and mass transfer rates. Typical examples are corrugated surfaces encountered in condensers and evaporators, and structured packings used in absorption columns and distillation trays [Fair and Bravo (1990)].

Recent studies of film flow over wavy walls include asymptotic and numerical analyses in the limit of creeping flow [Wang (1981); Pozrikidis (1988); Shetty and Cerro (1993); Kang and Chen (1995)], linear analysis of finite Re number flow in the limit of corrugations of vanishing amplitude [Bontozoglou and Papapolymerou (1997)] and only two numerical computations of finite Re flow along large corrugations [Trifonov (1998); Malamataris and Bontozoglou (1999)]. There is also some activity in the related problem of film flow inside a cylindrical wall with periodic diameter modulations [Kouris and Tsamopoulos (1998)]. Experimental results for these flows are available only for highly viscous liquids and vanishing Re [Zhao and Cerro (1992); Shetty and Cerro (1993)].

There are some indications from the above studies that non-trivial modifications of the flow take place when inertia forces become significant. Bontozoglou and Papapolymerou (1997) predicted a weak resonant interaction resulting in stationary, free surface waves with amplitude more than twice the wall disturbance, for wall corrugations with wavelength around 2 mm and Re in the range 180-200. This resonance has been confirmed by a finite-element computation of the steady, developing flow over a large amplitude sinusoidal wall [Malamataris and Bontozoglou (1999)]. Trifonov (1998), computing by a spectral method the flow over sinusoidal waves with length $L = 1.57\text{ mm}$ and height $H = 0.175\text{ mm}$, predicted the existence of a re-circulation zone at the wall trough. This zone disappeared at an intermediate range of Re numbers (130 – 290) and, in the same range, the disturbance height at the free surface exceeded that of the wall.

Flow over a wavy bed has been studied thoroughly in terms of potential theory [Kennedy (1963)], motivated by the phenomena of dune formation during sediment transport in rivers and Bragg scattering of surface waves in harbors. When horizontal, uniform base flow with constant velocity U is considered, linear theory predicts that resonance takes place between a stationary free surface wave and the bottom forcing when

$$U^2 = \left(\frac{g}{k}\right) \tanh(kh) \quad (1)$$

Weakly nonlinear solutions have been computed [Mei (1969)] and their linear stability [Miles (1986)] and long-time evolution [Sammarco, Mei and Trulsen (1994)] have been investigated. Numerical results for the fully nonlinear problem [Bontozoglou, Kalliadas and Karabelas (1991)] have provided evidence for subharmonic resonances, where the dominant surface wave is one half and one third the bed wave.

The results of potential theory are not applicable to the laminar flow of thin films, as they do not account for the effect of gravity in the direction of flow and for the effect of viscosity, which is expected to be significant in the small geometric scale of the film flow problem. However, it is interesting to note that the notion of a wall/free surface resonance is a unifying feature of the two models.

In this paper, laminar film flow along a wall with large amplitude, periodic corrugations is studied. A numerical scheme is employed based on the streamfunction formulation and involving Fourier and Chebyshev expansions in the streamwise and normal directions respectively. The nonlinear extension of the resonance predicted by Bontozoglou and Papapolymerou

¹ Mechanical & Industrial Engineering, University of Thessaly, Pedion Areos, GR-38334 Volos, Greece

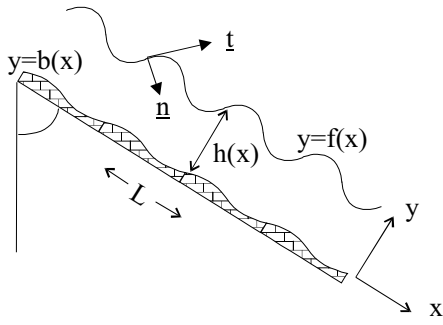


Figure 1 : Sketch of the flow with all the pertinent parameters.

(1997) is considered, and the effect of corrugation height is systematically investigated.

2 Problem formulation

Two-dimensional flow down a wall with an average inclination ϕ relative to the vertical direction is considered, with flow rate per unit span equal to q (Fig. 1). The wall has sinusoidal corrugations of wavelength L (wavenumber $k = 2\pi/L$), at right angles to the flow direction. The flow is described by a cartesian coordinate system, with the x axis in the streamwise and the y axis in the normal direction. The origin of the y -axis is set at the mean wall level, and the corrugations are described by the equation

$$y = b(x) \tag{2}$$

The free surface is assumed to be periodic and time-independent and to be described by the equation

$$y = f(x) \tag{3}$$

Physical constants of the liquid include the density, ρ , kinematic and dynamic viscosity, ν, μ and the surface tension, σ .

The streamfunction, ψ , is introduced, in terms of which the x and y velocity components are expressed as

$$u = \frac{\partial \psi}{\partial y} \tag{4}$$

$$v = -\frac{\partial \psi}{\partial x} \tag{5}$$

and the equation of motion becomes

$$-\frac{\partial \psi}{\partial x} \frac{\partial(\nabla^2 \psi)}{\partial y} + \frac{\partial \psi}{\partial y} \frac{\partial(\nabla^2 \psi)}{\partial x} = \nu \nabla^2(\nabla^2 \psi) \tag{6}$$

The no-slip and no-penetration conditions along the solid wall give

$$\psi = 0 \text{ on } y = b(x) \tag{7}$$

$$\frac{\partial \psi}{\partial \underline{n}} = \nabla \psi \cdot \underline{n} = 0 \text{ on } y = b(x) \tag{8}$$

where \underline{n} is the unit vector locally normal to the wall.

The kinematic boundary condition at the free surface requires

$$\psi = q \text{ on } y = f(x) \tag{9}$$

where q is the flow rate per unit span. The tangential and normal stress balance on the free surface are expressed in terms of the stress tensor, $\underline{\underline{\sigma}}$, as follows

$$(\underline{\underline{\sigma}} \cdot \underline{n}) \cdot \underline{t} = 0 \tag{10}$$

$$(\underline{\underline{\sigma}} \cdot \underline{n}) \cdot \underline{n} = -p_0 + \sigma \left[\frac{(d^2 f/dx^2)}{\{1 + (df/dx)^2\}^{3/2}} \right] \tag{11}$$

where

$$\underline{t} = \left(1, \frac{df}{dx} \right) / \sqrt{1 + (df/dx)^2} \tag{12}$$

$$\underline{n} = \left(\frac{df}{dx}, -1 \right) / \sqrt{1 + (df/dx)^2} \tag{13}$$

are unit vectors locally tangential and normal to the free surface. By expressing the rate of strain in terms of the streamfunction, Eq. 10-11 become

$$-\frac{\partial^2 \psi}{\partial y^2} + \frac{\partial^2 \psi}{\partial x^2} + 4 \frac{\partial^2 \psi}{\partial x \partial y} \left[\frac{(df/dx)}{1 - (df/dx)^2} \right] = 0 \tag{14}$$

$$p + \sigma \left[\frac{(d^2 f/dx^2)}{\{1 + (df/dx)^2\}^{3/2}} \right] + 2\mu \frac{\partial^2 \psi}{\partial x \partial y} \left[\frac{\{1 + (df/dx)^2\}}{\{1 - (df/dx)^2\}} \right] = 0 \tag{15}$$

Eq. 6 and boundary conditions Eq. 7-9, 14 and 15 are nondimensionalized using as characteristic length the inverse wavenumber of the periodic wall corrugations, $1/k$, and as characteristic velocity the product, kq . The following dimensionless numbers then appear:

$$Re = \frac{q}{\nu} \text{ Reynolds number} \tag{16}$$

$$Fr = \frac{k^3 q^2}{g_x} \text{ Froude number} \tag{17}$$

$$We = \frac{\sigma h}{\rho q^2} \text{ Weber number} \tag{18}$$

$$h_N = kh \text{ dimensionless Nusselt film thickness} \tag{19}$$

where h is the Nusselt film thickness, corresponding to laminar flow over a flat wall and given by

$$h = \left(\frac{3\nu q}{g_x} \right)^{1/3} \tag{20}$$

Term g_x is the component of gravity in the direction of flow. The dimensionless numbers are coupled through the expression

$$h_N = \frac{3Fr}{Re} \quad (21)$$

3 Numerical procedure

The problem formulated in section 2 is highly nonlinear and involves nonlinear boundary conditions on the free surface, whose location is not known a priori and has to be found as part of the solution. To circumvent this difficulty, a coordinate transformation is performed from the (x, y) to the (x, w) system, where the w coordinate is defined as

$$w = \frac{y - b(x)}{f(x) - b(x)} = \frac{y - b(x)}{h(x)} \quad (22)$$

and $h(x)$ is the local film thickness. Under this transformation, the wavy wall corresponds to $w = 0$ and the free surface to $w = 1$.

The stream function, $\psi(x, y) = \Psi(x, w)$, is expressed as a truncated Fourier series in the x -direction and as an expansion in Chebyshev polynomials in the w -direction:

$$\Psi(x, w) = \sum_{j=0}^m \sum_{k=0}^n \{a_{jk} \cos(kx) + b_{jk} \sin(kx)\} T_j(w) \quad (23)$$

The local film thickness is expressed as a truncated Fourier series

$$h(x) = \sum_{k=0}^n A_k \cos(kx) + B_k \sin(kx) \quad (24)$$

The coefficients of Eq. 23-24 are the unknowns in the numerical formulation. Taking into account that b_{j0} and B_0 are identically zero, the number of unknowns is $(2n + 1)(m + 2)$.

Derivatives of the streamfunction, $\psi(x, y)$, appearing in the differential equation and the boundary conditions, are expressed in terms of $\Psi(x, w)$ and $h(x)$ by application of the chain rule. For example,

$$\begin{aligned} \frac{\partial \psi}{\partial x} &= \frac{\partial \Psi}{\partial x} + \frac{\partial \Psi}{\partial w} \frac{\partial w}{\partial x} \\ \frac{\partial \psi}{\partial y} &= \frac{\partial \Psi}{\partial w} \frac{\partial w}{\partial y} \\ \frac{\partial^2 \psi}{\partial x^2} &= \frac{\partial^2 \Psi}{\partial x^2} + 2 \frac{\partial w}{\partial x} \frac{\partial^2 \Psi}{\partial x \partial w} + \frac{\partial^2 w}{\partial x^2} \frac{\partial \Psi}{\partial w} + \left(\frac{\partial w}{\partial x} \right)^2 \frac{\partial^2 \Psi}{\partial w^2} \end{aligned} \quad (25)$$

Derivatives of the new coordinate, w , are computed from Eq. 22 and Eq. 24. For example,

$$\begin{aligned} \frac{\partial w}{\partial x} &= -\frac{(db/dx)}{h(x)} - \frac{[y - b(x)](dh/dx)}{[h(x)]^2} \\ \frac{\partial w}{\partial y} &= \frac{1}{h(x)} \end{aligned} \quad (26)$$

Particular attention is paid to the implementation of the normal stress boundary condition, Eq. 15, as the pressure is not directly calculated in the streamfunction formulation. The actual boundary condition implemented involves the *derivative* of Eq. 15 *along the free surface* set equal to zero. The derivative of the pressure (first term of Eq. 15) is calculated as,

$$\left(\frac{dp}{dx} \right)_{w=1} = \frac{\partial p}{\partial x} + \frac{\partial p}{\partial y} \left(\frac{dy}{dx} \right)_{w=1} = \frac{\partial p}{\partial x} + \frac{\partial p}{\partial y} \frac{df}{dx} \quad (27)$$

The partial derivatives of pressure in the cartesian coordinate system are now computed from the x - and y -component of the Navier-Stokes equation. This procedure amounts to a projection of the Navier-Stokes equation along the free surface (Pozrikidis, 1997). The second term of Eq. 15 can be routinely differentiated, whereas the chain rule – as applied in Eq. 27 – is again invoked when computing the derivative along the free surface of the expression $\partial^2 \psi / \partial x \partial y$, appearing in the third term of Eq. 15.

A collocation scheme is used for the numerical solution. The boundary conditions are applied at each point

$$x_k = 2\pi k / (2n + 1), k = 0, \dots, 2n \quad (28)$$

along the boundaries $w = 0$ and $w = 1$, and the differential equation in Eq. 6 is applied at points (x_k, w_j) , where

$$w_j = \frac{1}{2} \left[1 + \cos \left(\frac{\pi j}{m} \right) \right], j = 1, \dots, m - 1 \quad (29)$$

Included in Eq. 29 is a transformation mapping the $[-1, 1]$ domain of definition of the Chebyshev polynomials into $[0, 1]$ adopted for variable w . The above implementation results in $(2n + 1)(m + 4)$ equations, which exceed by $2(2n + 1)$ the number of unknowns. This is a common problem with spectral methods and is presently overcome by discarding two rows of collocation points around $w = 0.5$.

The resulting system of algebraic equations is solved by Newton's method, in double precision arithmetic. The Jacobian matrix of the partial derivatives is calculated numerically for each iteration. Convergence is quadratic and 4 – 6 iterations are usually enough to bring residues down to 10^{-13} . Accuracy is tested by confirming independence of the results on the number of terms retained in Eq. 23-24. The magnitude of error can typically be monitored by the ratio of the last to the largest coefficient in the x and w expansions.

As expected, higher wall corrugations demand more Fourier harmonics for correct representation of the flow field. The majority of the results is computed using 15 harmonics and the ratio of last to largest coefficient is in the range $10^{-8} - 10^{-10}$.

The number of Chebyshev polynomials needed has a more peculiar behavior. Twenty terms have been used throughout the calculations and seem to give accurate results irrespective of the degree of nonlinearity of the wall corrugations. (Calculations with thirty terms have been performed and agreement

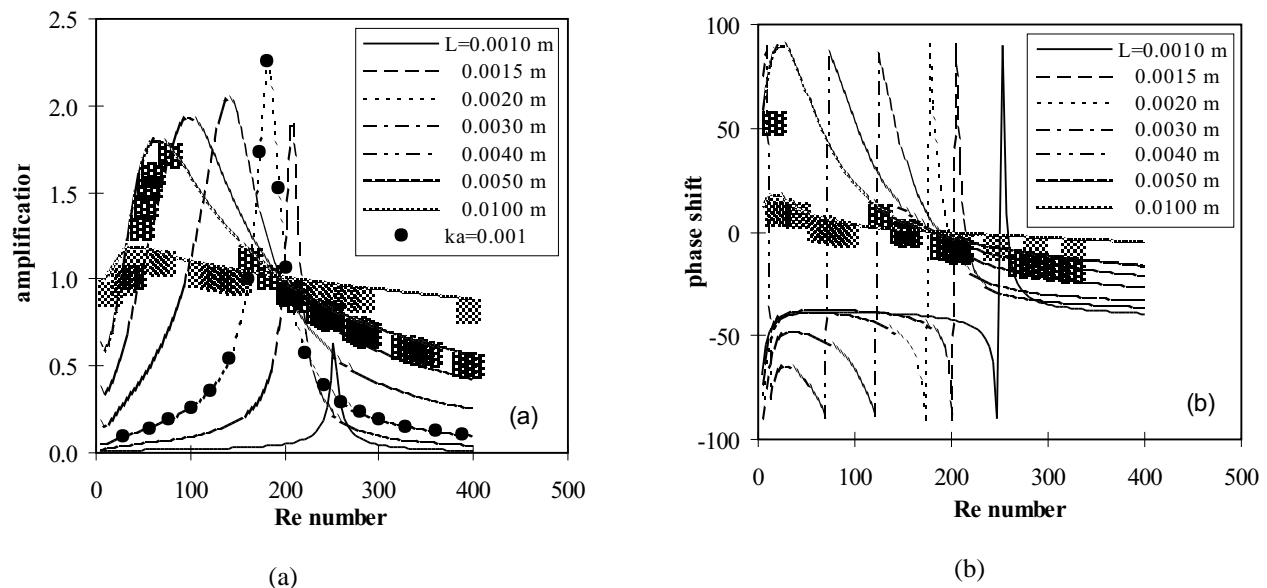


Figure 2 : Free surface amplification (a) and phase shift (b) of a sinusoidal wall disturbance, as predicted by linear theory for $\phi = 60^\circ$ and seven different wavelengths. Points are results computed using the numerical scheme with $ka = 0.001$.

to the fourth decimal figure is attained) However, using significantly fewer than 20 terms (for example, 10) produces in some cases erroneous results even in the limit of wall with small amplitude waves. In these problematic cases, the iteration converges normally and the ratio of last to largest coefficient is in the deceptively comfortable range $10^{-2} - 10^{-3}$. Thus, a ratio of $10^{-6} - 10^{-7}$ is used as a safe criterion.

Accuracy of the numerical scheme is confirmed by two tests. First, a very small wall amplitude is used ($ka = 0.001$) and the linear resonance curve is fully recovered. The agreement is demonstrated in Fig. 2a, where numerical results are shown as points. A second test is the duplication of representative results of Trifonov (1998), concerning the flow of liquid nitrogen over a sinusoidal wall with specific dimensions. The streamline patterns of the two computations turn out to be visually indistinguishable.

4 Results

4.1 Small corrugations

In the limit of small sinusoidal corrugations, the problem can be linearized and solved semi-analytically. This study has been presented elsewhere [Bontozoglou and Papapolymerou (1997)] but the key results are recounted here in order to bring out the physical implications and to provide background for investigating the nonlinear case.

Linear analysis predicts a free surface profile with the same wavelength as the wall corrugations, but different amplitude and phase. The amplification, defined as the ratio of free surface to wall amplitude, and the phase shift are presented in

Fig. 2a and 2b respectively, for water flowing along a wall inclined by 60° with respect to the vertical. These results are also valid for all other inclinations, as the effect of inclination was found to be insignificant unless the channel becomes nearly horizontal. The physical properties used in the computation are $\rho = 1000 \text{ kg/m}^3$, $\mu = 0.001 \text{ kg/ms}$, $\sigma = 0.072 \text{ N/m}$ and results are plotted for seven different wavelengths in the range $0.01 - 0.001 \text{ m}$.

The most interesting behavior appears for wavelengths around 0.002 m . Significant amplification is calculated for a short range of Re numbers, while a jump in the phase shift – depicted in Fig. 2b – indicates resonant interaction. The amplification pattern presented in Fig. 2a shows that, for shorter waves, the resonant behavior decreases in intensity and is conveyed to higher Re . For longer waves, the interaction moves to lower Re and loses its sharpness. It is finally noted that the linear amplification is always finite, indicating a weak resonance. The small characteristic length predicted by linear theory to have the strongest interaction indicates the importance of wall microstructure in modifying the film flow. In this context, it is of interest to note that structured packings and other corrugated surfaces encountered in process equipment, possess small-scale structure of similar dimensions, which has been shown in practice to have a significant effect on their performance [Fair and Bravo (1990)].

4.2 Free surface profiles over corrugations of finite amplitude

Linear analysis indicated that the most pronounced wall/free surface interaction occurs for wall corrugations with length

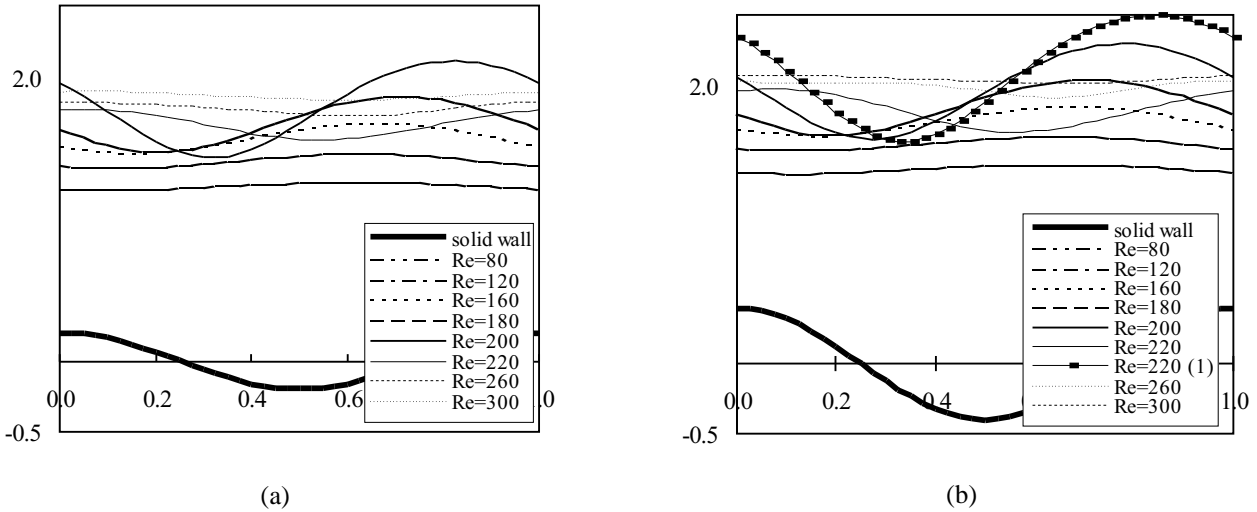


Figure 3 : Free surface profiles for wall corrugations with dimensionless amplitude $ka = 0.2$ (a) and 0.4 (b).

around 0.002 m . The rest of our study is devoted to nonlinear phenomena related to sinusoidal corrugations of this length and of finite height. The free surface profile and the structure of the flow are investigated for corrugations of varying amplitude. The shape of the free surface is roughly sinusoidal with amplitude and phase that depend on the Re number of the flow. The intensity of the free surface disturbance is again quantified by the amplification factor.

Representative free surface profiles are depicted in Fig. 3a-b for various values of Re number. Two sets of data are presented, corresponding to dimensionless wall amplitude $ka = 0.2$ (3a) and 0.4 (3b). The shift in phase associated with crossing of resonance conditions is observed in both cases. Thus, the free surface is almost 180° out-of-phase with the wall at sub-critical Re and almost in-phase at supercritical Re (actually, in both cases the free surface somewhat anticipates the wall).

Focusing on the wave amplitudes in Fig. 3a-b, we observe that the free surface is almost flat in the limit of low and high flow rates, but it is highly disturbed around $Re = 180 - 220$ (the curve marked as $Re = 220$ (1) in Fig. 3b corresponds to the upper branch in a Re range where the solution is triple-valued, as shown next). By comparing Fig. 3a and 3b, however, it becomes evident that the deflection of the free surface does not increase in proportion with the steepness of the wall corrugations for the highly corrugated walls considered. This is a manifestation of a feature of the flow structure to be considered in the next section.

The complete nonlinear resonance curve is produced by considering a specific corrugated wall and then computing the amplification for a wide range of flow rates. Such results (amplification vs. Re) are presented in Fig. 4 for dimensionless wall amplitudes $ka = 0.1, 0.2$ and 0.4 . All curves are skewed toward high Re numbers. For large amplitude corrugations,

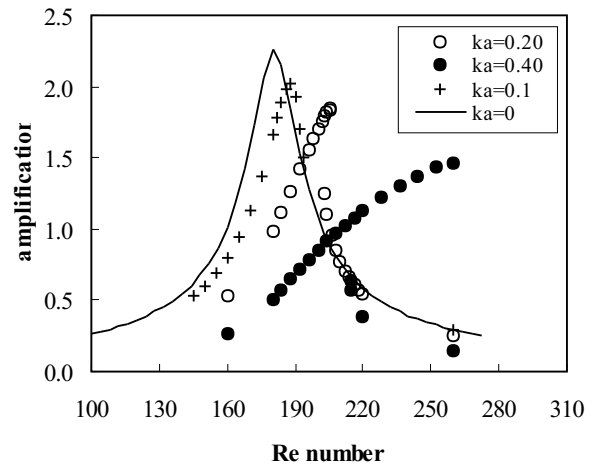


Figure 4 : Resonance curves for wall corrugations with dimensionless amplitude $ka = 0.0, 0.1, 0.2$ and 0.4 .

there exist two turning points, and the solution is triple-valued between them, as is typical of nonlinear resonance phenomena (the middle branch has not been computed). The turning points are expected to coalesce with decreasing wall steepness and, indeed, the resonance curve is single valued for $ka = 0.1$ and becomes triple-valued for ka slightly below 0.2 .

4.3 Structure of the flow over finite amplitude corrugations

The shape of the free surface discussed in the previous section provided information about the intensity of the nonlinear wall/free surface interaction. Further characteristics of the

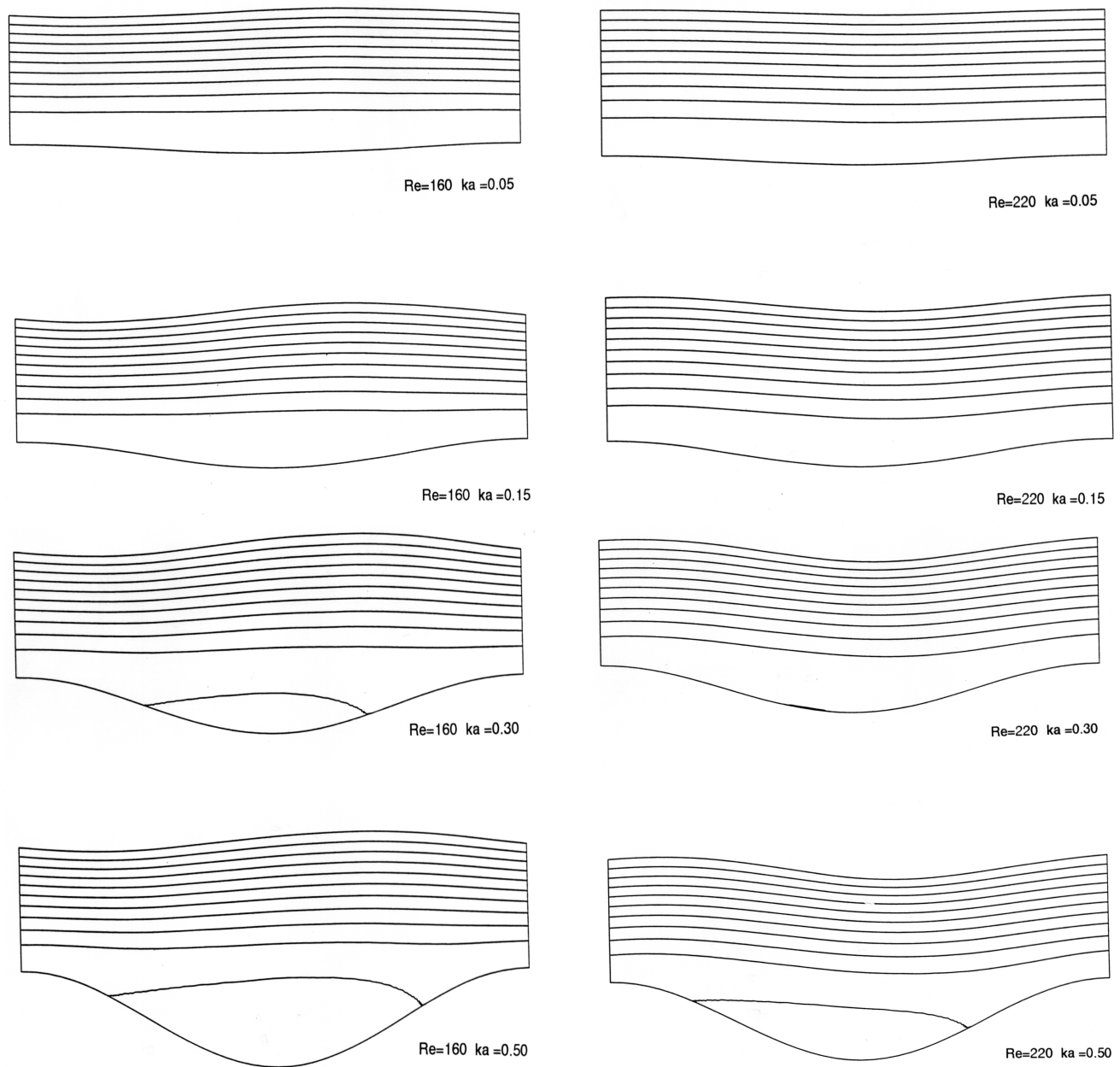


Figure 5 : Evolution of streamline patterns with Increasing corrugation steepness for $Re = 160$ and $Re = 220$.

flow are revealed by considering its structure in more detail. Streamline patterns, shear stress distribution at the wall and velocity variations close to the interface are examined.

Changes of flow structure with increasing wall height are shown in two series of streamline plots ($Re = 160$ and 220 respectively) in Fig. 5. In both cases, the flow close to the wall goes through the following stages. For corrugations of small amplitude, streamlines roughly follow the shape of the boundary. With increasing amplitude, the flow decelerates at the trough of the waves, as indicated by the increasing dis-

tance separating consecutive streamlines. A steep wall results in flow separation and formation of a recirculating zone, which extends farther from the wall as the corrugations become steeper.

The difference between the subcritical ($Re = 160$) and the supercritical ($Re = 220$) flow structure is mainly in the appearance and the extent of the separation zone and is related to the difference in the free surface patterns. Thus, for $Re = 220$ the free surface is roughly in-phase with the corrugations and, in

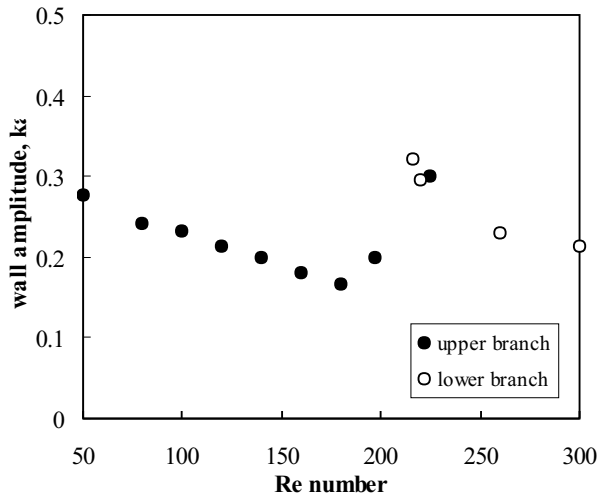


Figure 6 : Minimum wall steepness for separation to occur as a function of Re number.

this way, counterbalances the deceleration caused by the wall trough and delays separation. The opposite effect is caused by the out-of-phase free surface in subcritical flow, which leads to earlier separation and a more extensive recirculation zone.

In both cases, once formed, the separation zone grows with increasing corrugation height and thus acts as a buffer between the wall and the flow, minimizing the additional effect of very steep corrugations. This behavior offers an explanation for the previously observed insensitivity of the free surface to corrugation height for very steep corrugations (Fig. 3a-3b).

The minimum corrugation amplitude leading to separation is shown for several values of Re number in Fig. 6. As generally expected, inertial effects promote the appearance of separation. This is indicated on the left and right side of Fig. 6, where the minimum wall amplitude for flow separation is seen to decrease with Re . However, separation is also postponed around the resonance conditions, as is indicated by the central part of the figure. As previously noted, the solution is triple-valued in a region of Re around resonance, and the two curves in Fig. 6 – which cross at $Re = 222$ – correspond to the upper and lower branch of this solution. Thus, it is seen that resistance to separation is a common feature of both branches.

The observation that flow separation is postponed for a range of Re numbers was first made by Trifonov (1998), who computed the flow of liquid nitrogen ($\rho = 808 \text{ kg/m}^3$, $\mu = 0.0001147 \text{ kg/ms}$, $\sigma = 0.00887 \text{ N/m}$) over sinusoidal corrugations with length $L = 1.57 \text{ mm}$ and amplitude $a = 0.0875 \text{ mm}$ ($ka = 0.35$). He found that there is no separation for Re number in the range 130 – 290, which is a wide range around the resonance for his system parameters. It is noted that the values

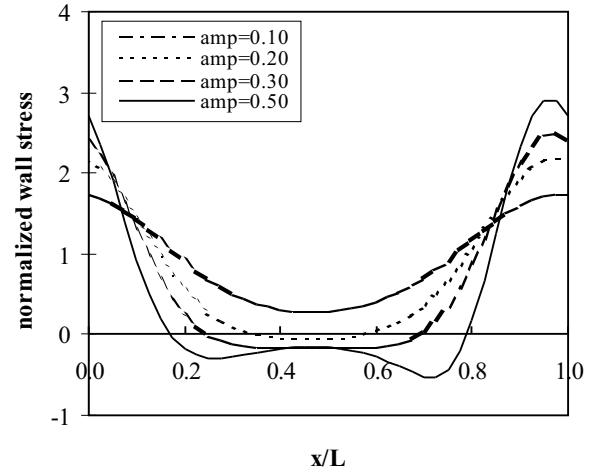


Figure 7 : Shear stress distribution along the wall for $Re = 160$.

of viscosity and surface tension used in Trifonov's computation are an order of magnitude smaller than the respective values for water, and it has been demonstrated that both these factors tend to suppress flow separation [Malamataris and Bontozoglou (1999)].

The distribution of shear stress along the wall is studied next. Wall shear stress is important in processes involving heat and mass transfer to or from the wall. Also, during material dissolution or deposition, wall shear stress determines the shape of emerging patterns. A typical shear stress distribution is presented in Fig. 7 for $Re = 160$ and for various wall amplitudes. In all cases, the values are normalized with the stress for the same flow conditions but for a perfectly plane wall.

The overall behavior is qualitatively attributable to the acceleration and deceleration of the fluid above the crest and trough respectively. It can be anticipated by simple mass conservation arguments, on the assumption that the presence of the free surface does not greatly affect the flow in the vicinity of the wall.

With increasing amplitude, separation and flow reversal at the trough are manifested by the appearance of negative stress values, while the maximum close to the crest becomes steeper. Finally, at very high amplitude, a secondary pattern develops in the recirculating zone, involving two local maxima in the absolute value of shear stress, located roughly symmetrically with respect to the trough.

The distribution of fluid velocity at the free surface is considered next. It has been argued in the literature that liquid fluctuations very close to a gas/liquid interface determine the rate of absorption of sparingly soluble gases [McCready and Hanratty (1985); Magnaudet, George, Masbernat, and Caus-

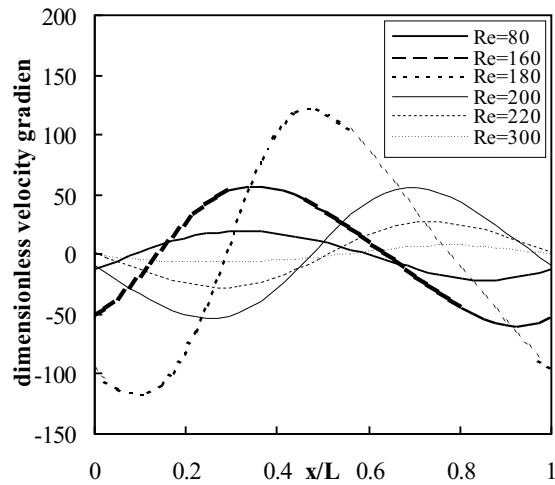


Figure 8 : Distribution of dimensionless normal velocity gradient along the free surface for small-amplitude corrugations and various Re numbers.

sade(1990); Jahne (1990)]. Gas absorption is a phenomenon of great importance in many industrial processes aiming at pollution abatement, and in environmental phenomena such as oxygenation of water masses and global CO_2 recirculation. The thickness of the concentration boundary layer of this mass transfer problem is known to be very small, typically on the order of $10 - 200 \mu m$. Because of this, the velocity component normal to the interface dominates mass convection. Given that for time independent flows the normal velocity is zero right on the interface, it can be locally represented by a Taylor expansion in the distance, y , from the interface

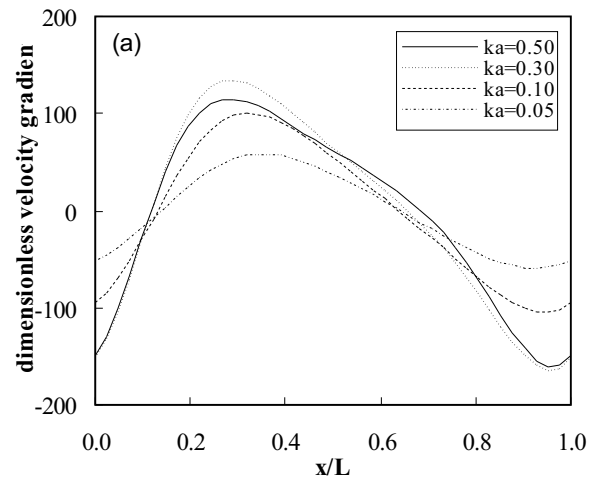
$$v = \beta y + O(y^2) \tag{30}$$

In the general case of a curved interface, β is the directional derivative (normal to the interface at $y = 0$) of the normal component of the velocity. It can be calculated from the expression

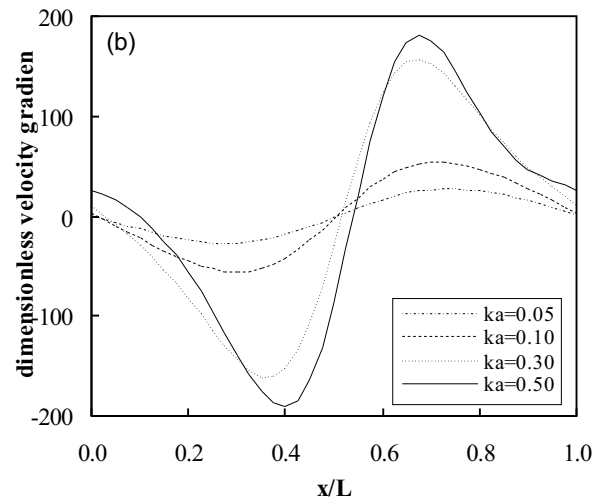
$$\beta = \nabla(\underline{u} \cdot \underline{n}) \cdot \underline{n} \tag{31}$$

where \underline{u} and \underline{n} are the velocity vector and unit normal to the free surface respectively.

Results for term β are presented in Fig. 8 and 9a-b. Fig. 8 shows the distribution of β along the free surface for the weakly nonlinear case, $ka = 0.05$, and various Re numbers. Positive values correspond to inflow from the interface towards the bulk of the liquid, and negative values to the reverse direction. All curves are roughly sinusoidal – indicating small departure from linear behavior – and combination of an inflow and an outflow region occurs over each wavelength. The location of inflow lags by roughly 90° behind the wall phase



(a)



(b)

Figure 9 : Distribution of dimensionless normal velocity gradient along the free surface as a function of corrugation steepness for $Re = 160$ (a) and 220 (b).

at subcritical Re , and is shifted to 270° at supercritical Re . Approach of the resonance conditions is seen to intensify the velocity disturbance. The effect of nonlinearity is shown in Fig. 9a-b for $Re = 160$ and 220 respectively. In both cases, inflow and outflow maxima are seen to reach plateau values at intermediate wall amplitudes, and remain unaffected by further increase of the corrugation height.

A gradual expansion of the inflow region is evident with increasing amplitude for $Re=160$, with loss of the sinusoidal

shape and appearance of an inflow “shoulder”. These features can be qualitatively explained by inspection of the streamline pattern for high wall amplitudes (Fig. 5). With the growth of the recirculation zone, there are two locations along a wavelength where the flow decelerates and develops a component towards the wall. One is at the beginning of the trough and the second in the neighborhood of flow reattachment. The latter seems to coincide with the shoulder in Fig. 9a. The velocity pattern at $Re = 220$ – which is typical of the supercritical behavior – can be understood by referring to the respective streamline plot (Fig. 5). In particular, the deflection of the free surface over the trough, in combination with the stagnation zone, create a restriction followed by an expansion of the active flow cross-section. This modification is believed to result in the extensive outflow and then inflow regions at the free surface.

5 Concluding remarks

Laminar, gravity driven flow of a liquid down an inclined wall with sinusoidal corrugations is studied. The approach is numerical, through a spectral spatial discretization method involving Fourier modes in the streamwise direction and Chebyshev polynomials across the film. The problem is formulated using boundary-fitted coordinates, and steady solutions are obtained for corrugations of large amplitude.

The synchronous resonance between wall and free surface is investigated for corrugations with length 0.002 m , which – according to linear theory – lead to the strongest interaction. Nonlinear resonance curves, including a triple-valued range, are computed and the free surface profile is shown to be highly disturbed around resonance and to change in phase when switching from subcritical to supercritical flow.

Flow separation, resulting in the formation of a recirculation zone inside the wall trough, is computed for high enough corrugations. Separation is shown to occur easier and be more extensive at subcritical flows. The minimum corrugation height for separation to occur generally decreases with Re number, but attains larger values around the resonance conditions.

Shear stress distribution at the wall is shown to deviate significantly from the flat film flow, a result with implications for various wall-to-fluid transport processes. The spatial distribution of velocity gradient normal to the free surface is computed and regions of inflow (from free surface to the bulk) and outflow are identified. These results are of interest in determining heat and mass transfer rates in process equipment involving gas-liquid flow.

The stability of presently computed steady solutions is a question open for research. Intuition, based on available results of film flow over a plane wall, leads one to expect that this flow will also become unstable beyond a Re number. It is, however, expected that salient features of the steady solutions presently computed will persist in the more complex time-dependent

flow.

References

- Benjamin, T. B.** (1957): Wave formation in laminar flow down an inclined plane. *J. Fluid Mech.*, vol. 2, pp. 554–574.
- Benney, D. J.** (1966): Long waves on liquid films. *J. Math. and Phys.*, vol. 45, pp. 150–155.
- Bontozoglou, V.; Kalliadasis, S.; Karabelas, A. J.** (1991): Inviscid free-surface flow over a periodic wall. *J. Fluid Mech.*, vol. 226, pp. 189–203.
- Bontozoglou, V.; Papapolymerou, G.** (1997): Laminar film flow down a wavy incline. *Int. J. Multiphase Flow*, vol. 23, pp. 69–79.
- Chang, H.-C.** (1994): Wave evolution on a falling film. *Annu. Rev. Fluid Mech.*, vol. 26, pp. 103–136.
- Fair, J. R.; Bravo, J. L.** (1990): Distillation columns containing structured packing. *Chem. Eng. Prog.*, vol. 86, pp. 19–29.
- Fulford, G. D.** (1964): The flow of liquids in thin films. *Adv. Chem. Engng*, vol. 5, pp. 151–236.
- Jahne, B.** (1990): New experimental results on the parameters influencing air-sea gas exchange. In *Proceedings: Air-Water Mass Transfer*, pp. 593–607, Second Intl. Symp., U.S. Army Waterways Experimental Station/ASCE, Minneapolis.
- Kang, F.; Chen, K.** (1995): Gravity-driven two-layer flow down a slightly wavy periodic incline at low Reynolds numbers. *Int. J. Multiphase Flow*, vol. 21, pp. 501–513.
- Kennedy, J. F.** (1963): The mechanics of dunes and antidunes in erodible-bed channels. *J. Fluid Mech.*, vol. 16, pp. 521–544.
- Kouris, C.; Tsamopoulos, J.** (1998): Two phase flow in a constricted tube: lubrication approximation. In *Proceedings: 4th Eur. Computational Fluid Dynamics Conf*, pp. 717–722, Athens, Greece.
- Magnaudet, J.; George, J.; Masbernat, L.; Caussade, B.** (1990): Turbulence level below the waves and its relation to absorption. In *Proceedings: Air-Water Mass Transfer*, pp. 582–592, Second Intl. Symp. U.S. Army Waterways Experimental Station/ASCE, Minneapolis.
- Malamataris, N. A.; Bontozoglou, V.** (1999): Computer aided analysis of viscous film flow along an inclined wavy wall. *J. Comp. Phys.*, vol. 154, pp. 372–392.
- McCready, M. J.; Hanratty, T. J.** (1985): Effect of air shear on gas absorption by a liquid film. *AIChE J.*, vol. 31.

- Mei, C. C.** (1969): Steady free surface flow over a wavy bed. *J. Engng Mech. Div. ASCE EM*, vol. 6, pp. 1393–1402.
- Miles, J. W.** (1986): Weakly nonlinear kelvin-helmholtz waves. *J. Fluid Mech.*, vol. 172.
- Pozrikidis, C.** (1988): The flow of a liquid film along a periodic wall. *J. Fluid Mech.*, vol. 188, pp. 275–300.
- Pozrikidis, C.** (1997): *Introduction to Theoretical and Computational Fluid Dynamics*. Oxford Press, New York.
- Sammarco, P.; Mei, C. C.; Trulsen, K.** (1994): Nonlinear resonance of free surface waves in a current over a sinusoidal bottom: a numerical study. *J. Fluid Mech.*, vol. 279, pp. 377–405.
- Shetty, S.; Cerro, R. L.** (1993): Flow of a thin film over a periodic surface. *Int. J. Multiphase Flow*, vol. 19, pp. 1013–1027.
- Trifonov, Y.-Y.** (1998): Viscous liquid film flows over a periodic surface. *Int. J. Multiphase Flow*, vol. 24, pp. 1139–1161.
- Wang, C.-Y.** (1981): Liquid film flowing slowly down a wavy incline. *AIChE J.*, vol. 27, no. 2, pp. 207–212.
- Yih, C.-S.** (1963): Stability of liquid flow down an inclined plane. *Phys. Fluids*, vol. 6, pp. 321–334.
- Zhao, L.; Cerro, R. L.** (1992): Experimental characterization of viscous film flows over complex surfaces. *Int. J. Multiphase Flow*, vol. 18, pp. 495–516.